Available online at www.sciencedirect.com

ScienceDirect

Procedia Structural Integrity 8 (2018) 452–461

Structural Integrity Procedia

www.elsevier.com/locate/procedia

AIAS 2017 International Conference on Stress Analysis, AIAS 2017, 6-9 September 2017, Pisa, Italy

NDT thermographic techniques on CFRP structural components for aeronautical application

V. Dattoma[a], R. Nobile[a], F.W. Panella[a], A. Saponaro[a]*

[a]*Department of Engineering for Innovation, University of Salento, Lecce 73100, Italy*

Abstract

This paper describes the application of active pulsed Thermography (PT) as a Non-Destructive Test (NDT) method for the investigation of CFRP aeronautical components. The analyzed specimens include T-shaped stringers, previously monitored by ultrasonic analysis, and laminated flat plates with internal production defects. Several set-up tests allowed to identify optimal configurations for the defect detection, according to specimen geometry and defect location. A custom post-processing algorithm has been developed to improve thermographic data for more precise defect characterization, whilst a successive full-field contrast mapping allows to achieve a reliable defect distribution map and a better definition on larger areas. Detection of defects was studied with a specific thermal contrast evaluation, with a suitable choice of undamaged reference area during the transient cooling phase. The influence of heating time and experimental set-up on the thermal contrast results has also been studied; moreover, the ability of thermographic technique to detect real small production defects with accuracy and reliability is verified for CFRP aeronautical components.

Peer-review under responsibility of the Scientific Committee of AIAS 2017 International Conference on Stress Analysis

Keywords: NDT; pulsed thermography; thermal contrast; real defects; CFRP aeronautical components.

1. Introduction

Defects can be introduced in composite materials during the manufacturing process or are developed during normal service life. The most common defects can be porosity, the presence of voids and cracks in the matrix and mostly delaminations (Bolotin, 1996; Mallick, 2008; Ghobadi, 2017). For these reasons, defect detection becomes a

* Corresponding author. Tel.: +39 (0)832 297786; fax: +39 (0)832 297768.
E-mail address: andrea.saponaro@unisalento.it

Peer-review under responsibility of the Scientific Committee of AIAS 2017 International Conference on Stress Analysis
10.1016/j.prostr.2017.12.045

critical activity to verify integrity of structural parts (Roth et al., 1997; Hendorfer et al., 2007; Almond et al., 2012). Active thermographic methods are now a promising technique to check the structural integrity of CFRP aeronautical components (Avdelidis et al., 2003; Mayr et al., 2010; Almond and Pickering, 2014); the methods differ in the type of excitation source and thermal response processing; transient thermography techniques analyze the thermal maps during the cooling phase, as recorded on component surface after it has been exposed to various types of thermal pulses. For pulsed thermography (Maldague, 2003; Ibarra-Castanedo, 2005; Sun, 2006), adopted in particular in this work by the authors, halogen lamps are used to stimulate the inspected material with an unique intense thermal input. Unlike flash thermography (Maldague, 1993), thermal energy is applied for a longer time period and the presence of defects and their characteristics are analyzed by means of thermal contrast evaluation between non-defective zones and damaged areas (Maldague, 2003; Maldague et al., 2002).

The present work applies pulsed thermography (PT) to CFRP aeronautical components in the form of stringers and flat plates containing real defects, whilst in previous papers the authors applied similar techniques to detect artificial defects (Carofalo et al., 2012-2014) in composites. In addition, an extensive experimental campaign is needed to define the optimal set-up and optimization of parameters for a better detection and characterization of defects.

A matlab routine is developed by implementing Source Distribution Image methods (Susa et al., 2010), based typically on the analysis of isothermals to select a defect-free reference zone, supposing it receives the same heat flux of the damaged zone. In this paper a new method, based on algorithm named LBC *(Local Boundary Contrast)*, has been introduced by the authors; it is based on a new contrast mapping methodology, which allowed to achieve a better identification and more accurate distribution maps of dangerous defects.

2. Materials and specimens

The CFRP components investigated in this work include 2 T-shaped stringers (here denoted A and B) and 3 laminated flat plates. All specimens present different real defect typologies, such as slight and diffused delaminations with localized small voids in the first case and elevated porosity values in the latter case. The length of both stringers is 970 mm and their analysis has been performed inspecting the CAP areas, manufactured with Automated Tape Lay-up, with 15 plies and a thin protective tape on it for a thickness of 2.76 mm; the WEB zone is built with 30 plies and a total thickness of 5.20 mm, without protective tape (Fig.1a).

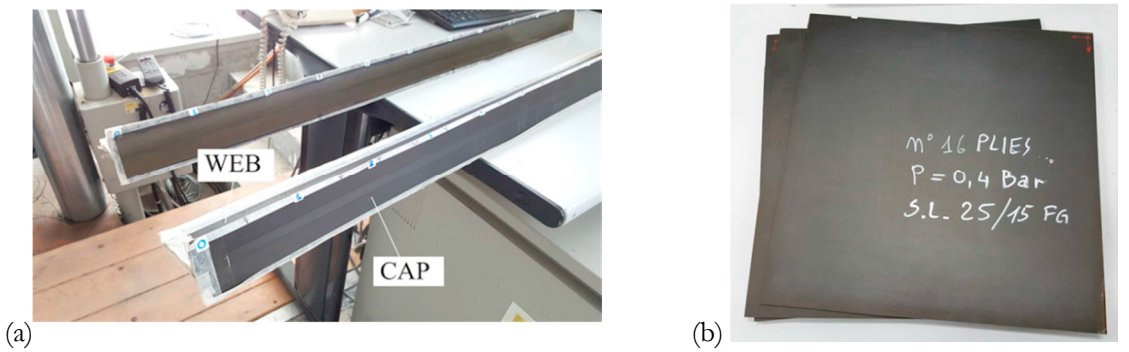

Fig. 1. (a) stringers parts inspected (CAP and WEB); (b) laminate flat plate specimens.

The flat plates (400 x 400 mm^2) have been manufactured in a vacuum bag in an autoclave (Fig. 1b), inducing porosity through pressure variation during curing cycles. The stacking sequence, number of plies and cure pressure for each plate are indicated in Tab. 1.

Tab. 1. Stacking sequence, number of plies and cure parameters of laminated plates.

Specimen	Thickness [mm]	No. of plies	Pressure [bar]	Stacking sequence
Panel 1	3.023	16	0.4	[0, +45, -45, 90, 0, +45, -45, 90]s
Panel 2	5.568	24	0.1	[0, +45, -45, 90, 0, +45, -45, 90, 0, +45, -45, 90]s
Panel 3	13.267	64	0,75	[0, +45, -45, 90, 0, +45, -45, 90]4s

3. Experimental setups and methods

3.1. T-shaped stringers

Several thermographic tests have been performed; the first ones are aimed at defining the optimal set-up for the detection of defects, improving uniform heat deposition on the whole surface. Successive different tests allowed to identify the optimal configurations for the CAP investigation on the stringer, with and without protective tape, as well as to define the best set-up for the WEB investigations. In particular, the first tests allowed to define a satisfactory configuration for the CAP inspection on stringer A, without protective tape; this efficient configuration includes the simultaneous activation of 4 halogen 1000 W lamps located 74 cm from the specimen and the camera at a distance of 42 cm (Fig. 2a). However, because of the critical geometry of the specimen which includes fillet zones and variable thicknesses, the edges of the stringers were masked with tape, and a support guide for their movement was applied to perform sequential analysis all along the stringer length.

Compared to set-up configuration No. 1 in Fig. 2a, a new optimum set-up arrangement is proposed in Fig. 2b, where the specimen is closer to the infrared camera and the four lamps were placed in a better position in terms of angles. For stringer B the infrared camera was rotated to avoid some reflections caused by the presence of protective tape and more tests allowed to achieve the best result as displayed in (Fig. 2c).

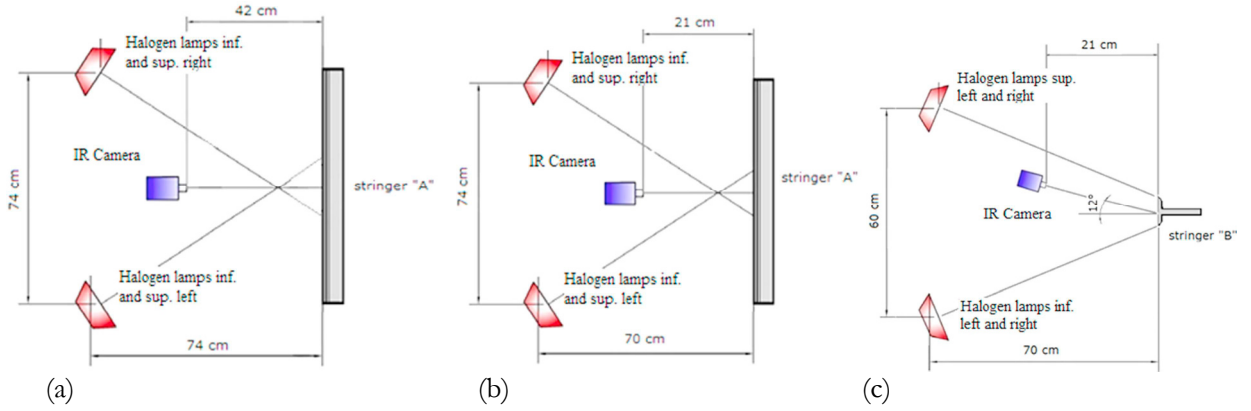

Fig. 2-a Top view of the initial configuration (No. 1); Fig. 2-b top view of configuration No. 2; Fig. 2-c lateral view of configuration No. 3, for both CAPs on inspection stringers A and B.

On the other hand, the WEB inspection required for both stringers the simultaneous use of only two halogen lamps to stimulate the component, with the thermal camera opportunely raised and rotated for a clear view due to CAP disturbance. The best distance of the lamps from specimens is approximately 85 cm, whilst the infrared camera is placed at a distance of 34 cm, as showed in Fig. 3.

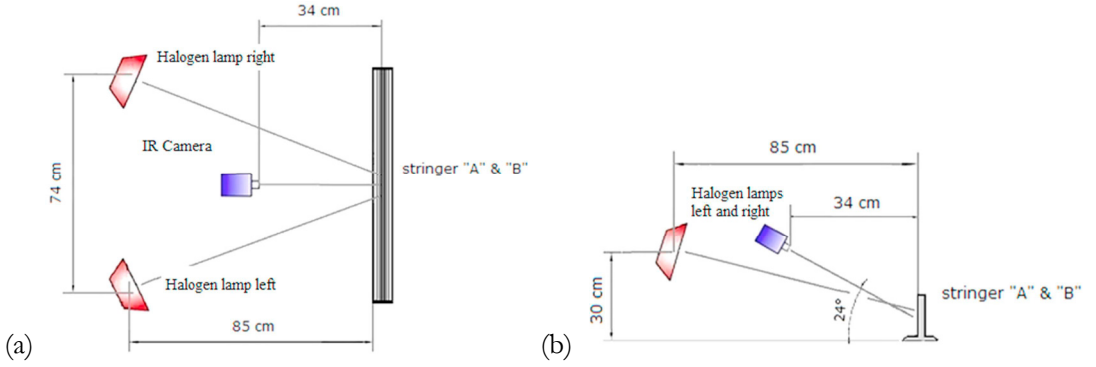

Fig. 3. Top view (a) and lateral view (b) of the thermographic configuration for the WEB inspection (stringer A and B).

Defect analysis was carried out with the camera and the light source on the same side by means of a FLIR 7500M IR camera, with a FPA cooled detector (Focal Plan Array), endowed with a NETD 25 mK InSb sensor and image resolution of 320 x 256 pixels; the halogen lamps were oriented differently and controlled by a signal generator connected to a dimmer power source for synchronizing time between the thermal pulse and the recording initialization. The thermographic investigation was performed by splitting the stringers in different sub-zones to inspect CAP and WEB (Fig. 4), in relation to the experimental set-ups. The first analysis zone is called zone a, the next one zone b and so on.

Schematic views (T-shaped stringers)	Dimension [mm]	
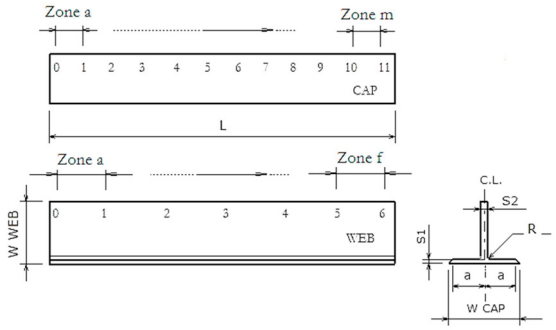	L (length)	970
	Zone a CAP	86
	Zone a WEB	148
	W CAP (CAP width)	59.3
	S1 (CAP thickness)	2.76
	W WEB (WEB width)	70
	S2 (WEB thickness)	5.20
	R (Radius)	3
	a	22.5

Fig. 4. Indication of the sub-zones scheme to investigate laminate areas (CAP and WEB).

A custom post-processing algorithm has been developed with matlab software for defect characterization; is starts with input of raw infrared camera data exported in ASCII format. Since ideal condition for thermal contrast calculation is verified when the undamaged zone is invested by the same heat flux of the defect, the elaboration depends on the choice the reference zone. SDI method (Susa et al., 2010) is a procedure initially implemented in this work, based on isothermal curves plots along which the reference areas and the defect zone are located. At the contrary, successive full-field contrast mapping methods allow to indicate directly the defect distribution on component surface. The algorithm gives the temperature variations, referred to defect free zones and the damaged areas. In this study the absolute and normalized thermal contrasts C_n and C_a are defined by formulae (1, 2). Subsequently the routine provides diagrams obtained during the transient cooling phase for the classic normalized contrast C_n and absolute contrast C_a:

$$C_a(t) = T_d(t) - T_i(t) \tag{1}$$

$$C_n(t) = (T_d(t) / T_d(t_0 + 1)) - (T_i(t) / T_i(t_0 + 1)) \tag{2}$$

where T is the temperature, t is the time instant chosen, while "d" and "i" refer to a defected and non-defected areas; t_0 is the instant when the heating ends. For both the thermal contrasts the algorithm computes two quantitative parameters connected to the defect characteristics: the maximum value of contrast C_{max} and the observation time tmax, when C_{max} is determined after the lamps are turned off.

Employing the initial set-up configuration in Fig. 2a, acquisitions were performed on stringer A with no protective tape, with two different heating times (3s and 5s) and 30s for acquisition of the cooling phase.

Adopting the configuration in Fig. 2b, a second series of acquisitions were performed on the entire stringer A, with various heating times (3s, 7s, 10s) on each single part of the CAP and a final one with a long heating time (t_{heat} =20s), only on damaged areas (found to be mainly on the outer stringer sides and the central zone), using a frame rate of 5Hz. Maintaining essentially the same configuration of stringer A, but with the IR camera opportunely oriented (Fig. 2c), we investigated the stringer B with protective tape; two tests were performed with heating times of 3s and 7s on the damaged areas and cooling acquisition times of 20s and 80s respectively.

On the WEB surfaces, three tests were performed for both stringers with the set-up described in Fig. 3, using three different heating times (7s, 10s and 20s) and cooling acquisition times of 80s, 120s and 300s respectively, with the same frame rate.

3.2. Laminated plates

Similarly to the stringers case, a new set-up for the defect investigation of CFRP plates was also studied. Four halogen lamps were used to stimulate the material. The distance between the specimen and the infrared camera was optimized at 73 cm and 100 cm from the lamps and Fig. 5 shows the experimental set-up used to inspect the specimens in the laboratory.

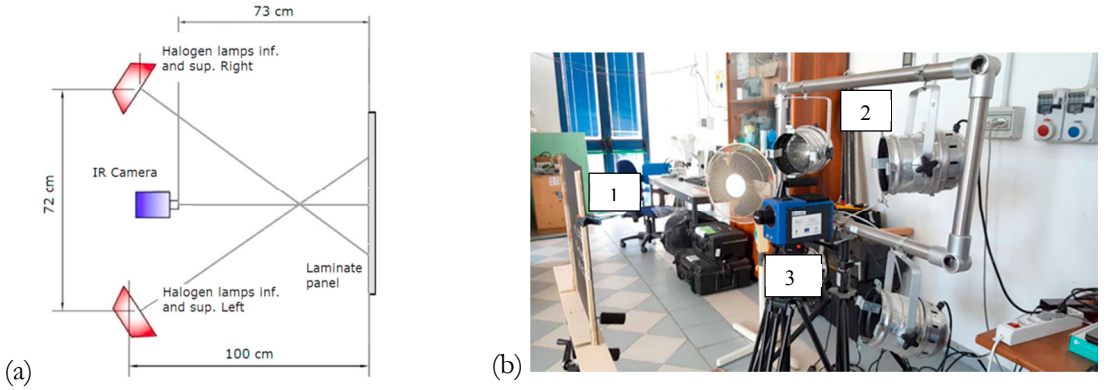

Fig. 5. (a), (b) Experimental set-up to investigate laminate plates. (1) Specimen, (2) lamps, (3) IR camera.

After first preliminary tests aimed at selecting the optimal set-up and thermal resolution, four new experiments were performed on two plates (16 and 24 plies) with different heating times (1, 5, 15, and 20s) and acquisition times of 60s, 80s, 120s and 150s, found to be within the optimized values for the given laminate thickness and material typology.

A second experimental configuration was examined by reducing the distance specimen/IR camera from 73 to 51 cm for better defect resolution, with the thermal camera placed behind the four lamps and a specimen/lamp distance of 48 cm. Four tests were performed on all three plates using different heating times from 1 to 20s for plate 1; from 10 to 50s for plate 2 and 3 to 40s for plate 3. In each test, a frame rate of 5Hz was used.

4. Discussion of results

4.1. Defect detection and analysis on T-shaped stringers

Many defect locations have been detected in the stringers; the most important and representative ones are indicated as defect d1 to d8 for simplicity. The analysis for defect d2 according to set-up configuration No. 1 is presented as an example for the investigated CAP of stringer A (Figs. 6a-d) in the left zone. In Figs. 8a-d, the complete analysis for other defects is represented, related to the investigation of the same stringer but with set-up No. 2 on the same CAP zone.

An heating time of 3s is found to be sufficient to detect defects, since thickness is small and carbon-based composites present higher heat transfer rates. In fact, the thermal maps and the isothermal plot in Fig. 6a at the beginning of the cooling phase present some hot spots even though temperatures are not perfectly uniform. In Fig. 6b, the thermal map shows the detected defects after 0.6s of cooling. Finally, figure 6c shows defect d2 in the same conditions and choice of defect free area based on isotherm curve analysis.

In Fig. 6d a temperature diagram is presented versus time, recorded for defect d2 and the related defect free zone, showing these defect characteristics produce very small contrast variations. The trend of the absolute and normalized contrasts (Carofalo et al., 2012) are illustrated in Figs. 7a-b; the absolute and normalized contrast curves are not regular, but present negative values due to fact that inversion time of 6,8s is quickly reached, beyond which the two curves are reversed (Fig. 6d). In general, some degree of heat accumulation is revealed during the heating phase, due to marginal defect depth.

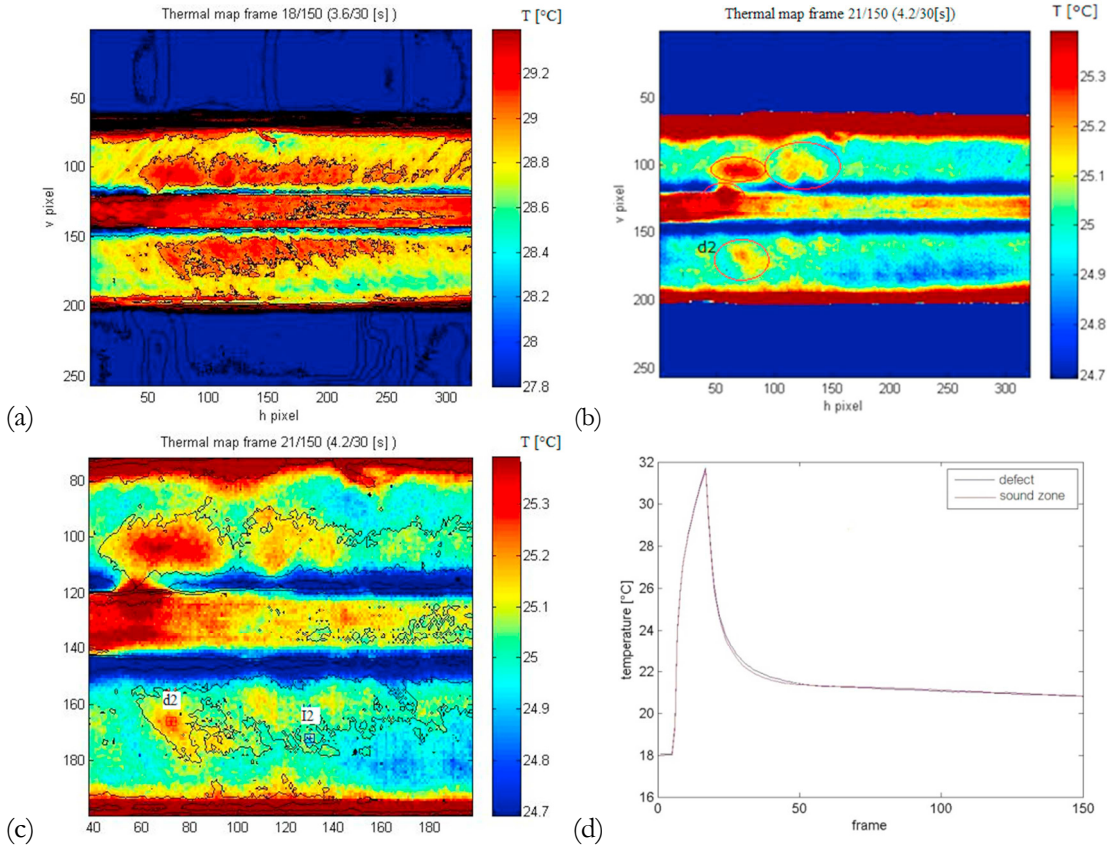

Fig. 6. (a) Maps of isotherms at the beginning of the cooling phase (heating for 3s); (b) thermal map recorded 0.6s after the lamps turning off (heating for 3s); (c) map of isothermal curves (zoom) recorded 0.6s after the lamps turning off (d2 processing defect, heating for 3s); (d) temperature vs. frame for defect d2 and non-defective zone. Configuration No. 1 for the CAP inspection on the stringer A, zone a.

From the normalized and absolute contrast curves in Fig. 7, an initial pre-heat storage of about 0.12 °C is evident for defect d2, while the maximum value of the absolute contrast $C_{a\,max}$ is equal to about 0.2 °C and related observation time $t_{a\,max}$ of about 1.4s from the lights turning off. The normalized contrast $C_{n\,max}$ has a maximum of 0.0026 °C and $t_{n\,max}$ of 1.4s.

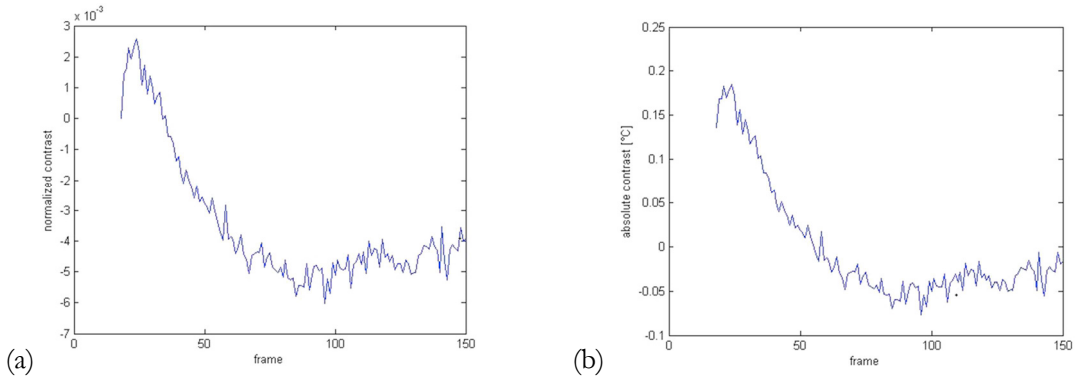

Fig. 7. The normalized contrast (a), and absolute one (b), for defect d2 during cooling (heating time 3s).

Figures 8a-d show the complete analysis for defects d1, d3 and d4 with set-up configuration No. 2 on the CAP in stringer A. The thermal map reported in Fig. 8a easily allows to distinguish the defects, some already detected with configuration No.1.

The $C_{a\,max}$ variations and $t_{a\,max}$ values versus the heating time for significant defects are shown in figure 8c-d.

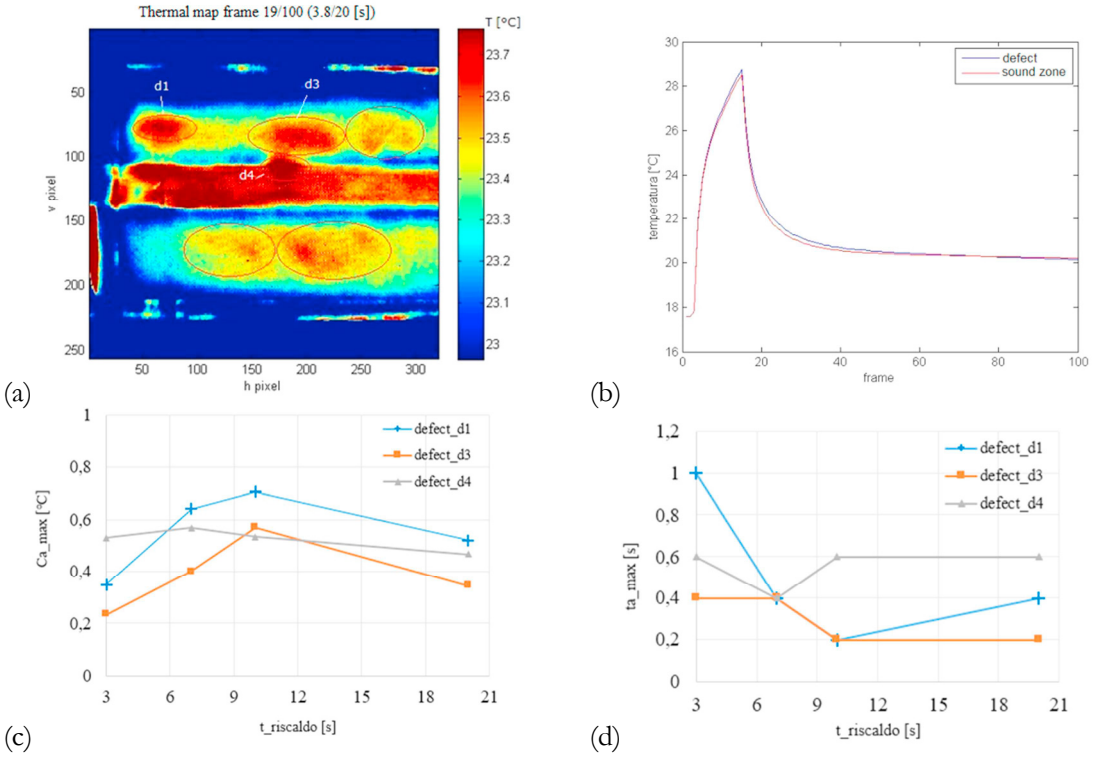

Fig. 8. (a) Thermal map recorded on stringer A, CAP "zone a" (configuration No. 2, with heating for 3s); (b) temperature vs. frames for defect d1 and in the non-defective zone; (c) behaviour of absolute contrast versus heating time, for defects d1, d3 and d4; (d) variation of the observation time versus heating time, for defects d1, d3 and d4.

Tab. 2. Summary table of first detected and characterized defects.

Defect	Configuration	Sub-zone	Ca_max [°C]	ta_max [s]	t_heat [s]	Specimen
d1	No. 2	Zone a CAP	0.7	0.2	10	stringer A
d2	No. 1	Zone a CAP	0.23	1.4	3	stringer A
d3	No. 2	Zone a CAP	0.571	0.2	10	stringer A
d4	No. 2	Zone a CAP	0.568	0.4	7	stringer A

In Table 2, the summarised information for defects d1-d4 is given. For defects d1 and d3 it may be observed that an increase of heating time from 3s to 10s will cause $C_{a\,max}$ to increase while $t_{a\,max}$ tends to decrease. consequently, by increasing the heating time, these defects are visible beforehand and with a higher contrast as expected. For heating times from 10s to 20s, $C_{a\,max}$ decreases (for defects d1 and d3) while the observation time increases for defect d1 and it remains constant for defect d2. Heating times up to 10s do not seem to be convenient for these defects because the sound area temperatures tend to reach the same temperatures of the defected zones; this explains the thermal contrast reduction. For defect d4 for instance, $C_{a\,max}$ increases from 3s to 7s where it assumes a maximum value of about 0.5 °C. Finally, the images in figure 9 show, as an example, more significative thermal maps on the stringer with protective tape (Fig. 9a) related to WEB "zone c" (stringer B mid-length) and also without protective tape (Fig. 9b) on WEB "zone a" (on the side of stringer A), in which some kinds of defects seem to be present.

On the WEB of both stringers, the optimal heating times for a good resolution of defect indication were different (7s, 10s and 20s). In all cases the defects are visible but with different contrast values, according to their width and location on the stringer length. Some areas on stringers revealed large defects in figure 9a, with a very low temperature intensity, difficult to characterize with precision because the related temperatures and contrast differences are too small with respect to defect free values and to data noise; only a check with destructive tests may establish the nature of these temperature variations. In table 3 there is a summary of other detected defects from d5 to d8, characterized in the same way for both stringers in other significant WEB and CAP locations.

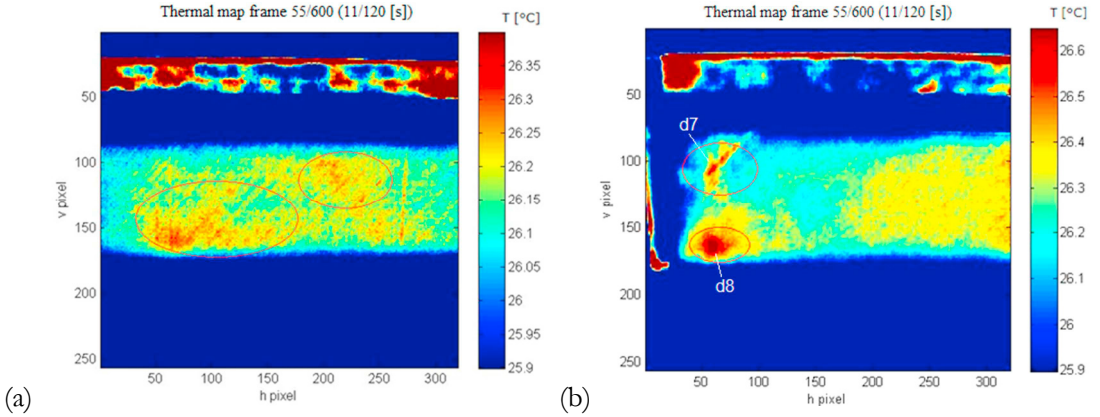

Fig. 9. (a) Thermal map recorded on the stringer B, WEB "zone c" (heating time 10s) with some degree of defect presence; (b) thermal map on the stringer A, WEB "zone a" (heating time 10s) with a clear example of dangerous defects.

Tab. 3. Summary table of other detected and characterized defects.

Defect	Configuration	Sub-zone	Ca_max [°C]	ta_max [s]	t_heat [s]	t_inv [s]	Specimen
d5	No. 2	Zone f CAP	0.228	0.4	3	6.6	stringer A
d6	No. 3	Zone f CAP	0.257	0.4	3	6.8	stringer B
d7	Web set-up	Zone a	0.307	0.4	10	17	stringer A
d8	Web set-up	Zone a	0.338	0.6	7	8.6	stringer A

Starting from the same temperature data, The full-field contrast mapping of more interesting acquisitions on selected stringer zones are achieved by means of the new processing algorithm LBC *(Local Boundary contrast);* on the CAP "zone a" of stringer A and CAP "zone f" of stringer B are displayed two interesting examples, in which it is possible to clearly distinguish the defect locations and boundary shape (Figs. 10a-b), giving better and immediate evidence of extension and distribution in the whole picture. The thermal contrast calculation was done basically considering the temperature differences in a suitable correlation window, centred on a selected corresponding location (using a 2D sub-matrix), weighted and subtracted by the mean temperature around the reference pixel. By iterating this procedure pixel by pixel on the whole frame in the routine and reprocessing the results in a new data matrix, it is possible to achieve a new temperature contrast mapping, here denominated LBC, within limited values. The results, after appropriate modification of the algorithm and parameters optimisation, are encouraging and are in accordance to results obtained during the previous thermographic inspection. In addition, this method immediately gives the whole map of the detected defects and revealing exact locations in an absolute modality, even for defects of different extensions and depths.

Finally, a microscopic analysis with the stereomicroscope performed on a stringer section allowed to observe the details and depths of internal voids that result to be confrontable with data emerged from thermographic inspection.

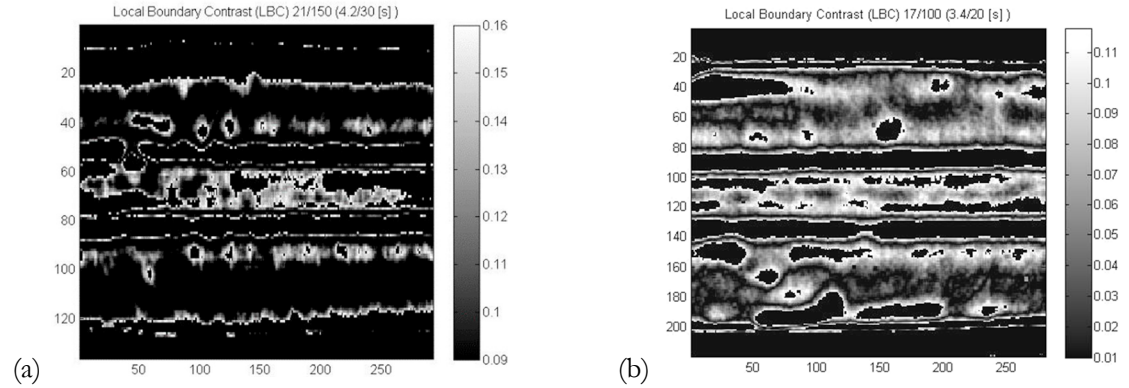

Fig. 10. Contrast mapping with LBC method: (a) defects d1 – d4 with heating time 3s for the CAP inspection stringer A, (b) other detected defects with heating time 3s for the CAP inspection stringer B on zone f.

4.2. Defect detection and analysis on laminated plates

Figure 11a shows the 8 defects detected in the central zone of the plate with 16 plies, while no test allowed to identify any defects in the plate with 64 plies with both adopted setups (Fig. 5). A brief thermal excitation appears adequate to limit the pre-heating effects of defects. In figures 11b-d, the analysis of defect d1 is presented as an example.

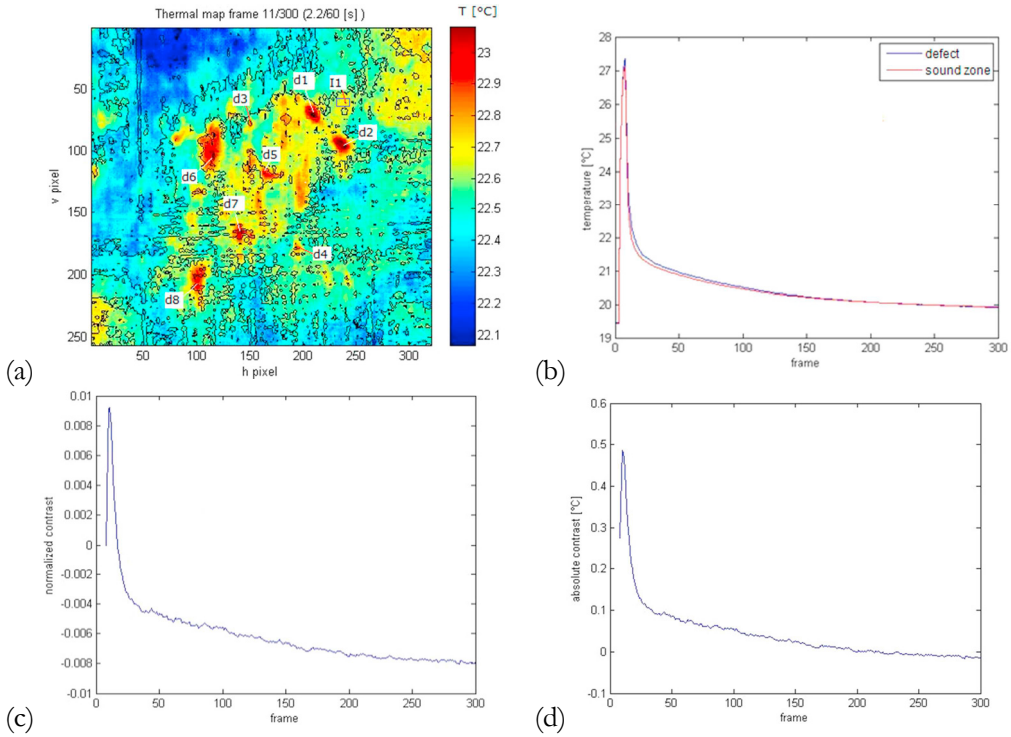

Fig. 11. (a) Thermal map recorded 0.8s after the lamps were turned off on the plate with 16 plies (heating for 1s); (b) temperature vs. frame for defect d1 and non-defective zone; trends of the normalized (a) and absolute (b) contrast, for defect d1.

An heating time of 1s is sufficient to detect the sub-superficial defects on the plate with 16 plies. Similar results were obtained on the plate with 24 plies. During the processing phase, particular attention was paid to the choice of the defect free reference zone for each defective part. These results show the pulsed thermographic technique is also suitable to detect porosity zones when present in substantial way.

In Fig. 12, the maximum absolute contrast and observation time versus the heating time are illustrated for defect zones d1-d8, as an example on the plate with 16 plies. Absolute contrast linearly increases, while observation time decreases when heating time arises. Consequently every defect is visible with a greater contrast.

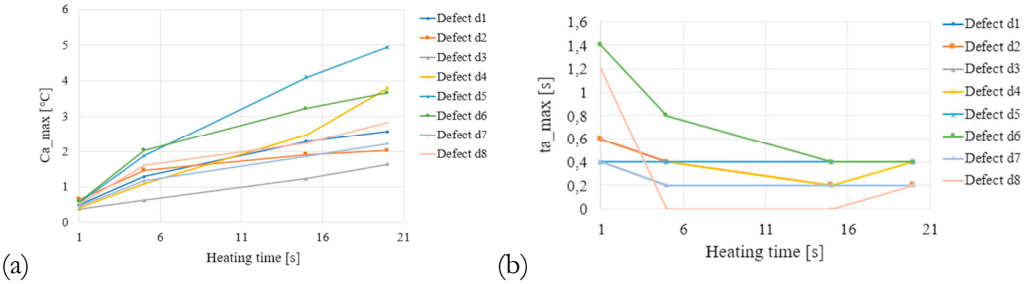

Fig. 12. (a) Absolute contrast to maximum versus heating time, for defects d1-d8; (b) observation time versus heating time, for defects d1-d8.

Internal defects at higher depth were observed on both plates of 16 and 24 plies with the optimal configuration; Figure 13a shows the thermal image zoom in a damage region after longer cooling (72.4s) on the plate with 24 plies, while the example of the thermal profile for defect d9 is shown in Figure 13b.

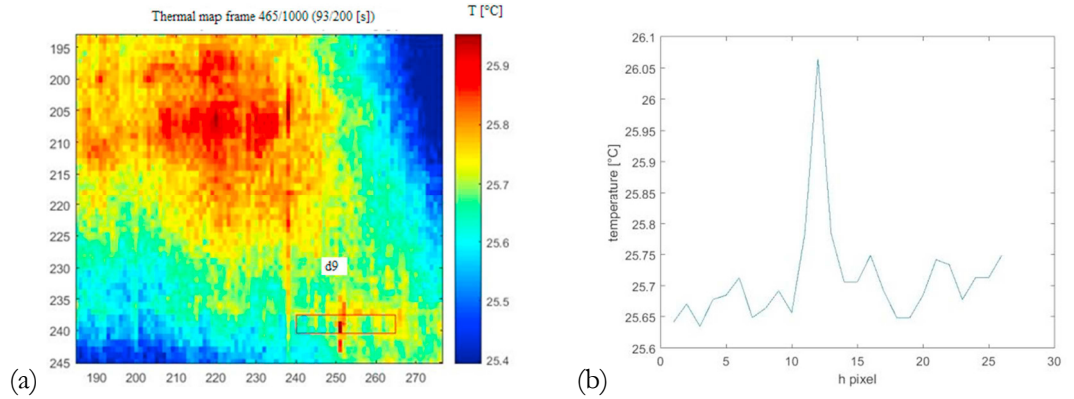

Fig. 13. (a) Thermal map recorded 72.4s after the lamps were switched off on the plate with 24 plies (heating time 20s); (b) thermal profile for defect d9.

Conclusions

The performance of pulsed thermographic method as Non-Destructive control applied to modern CFRP aeronautical components was optimised for optimal experimental set-up and data processing, in order to detect also small voids in the delamination zones.

Results show the optimised pulsed technique is extremely valid to detect with accuracy the real production defects on typical CFRP aeronautical components; in particular, the classical contrast parameters appear to give satisfactory results and all defects are easily detected, but these calculations are locally conducted and are expressed in a relative scale. By using a new algorithm, is possible to manipulate data for a full-field analysis and present a map of results on the specimens, in which defect boundaries are easily detected with respect to each other and according to their extension.

Acknowledgements

This work has been financially supported by the project PON03PE_00067_2 Defect, damage and repair techniques in the manufacturing process of large composite structures (DITECO).

References

Almond D.P., Pickering S.G. (2012) An analytical study of the pulsed thermography defect detection limit. J Appl Phys 111(9):093510.
Almond D.P., Pickering S.G. (2014) Analysis of the defect detection capabilities of pulse stimulated thermographic nde techniques. AIP Conf Proc 1581(1):1617–1623.
Avdelidis N.P., Hawtin B.C., Almond D.P., "Transient thermography in the assestment of defects of aircraft composites", NDT&E International, Vol. 36, 433-439 (2003).
Bolotin V.V. (1996) Delaminations in composite structures: its origin, buckling, growth and stability. Compos Part B: Eng 27(2):129–145.
Carofalo A., Dattoma V., Palano F., Panella F.W., "Rilevazione di Difetti in Compositi GFRP mediante Termografia Pulsata e Lock-In" XXXXI Convegno Nazionale Aias – Vicenza – 5-8 settembre 2012.
Carofalo A., Dattoma V., Palano F., Panella F.W., "ND Testing Advances on CFRP with Ultrasonic and Thermal Techniques" ECCM 16-16TH European Conference on Composite Materials, Seville, Spain, 22-26 June 2014.
Ghobadi, A. (2017) Common Type of Damages in Composites and Their Inspections. World Journal of Mechanics, 7, 24-33.
Hendorfer G., Mayr G., Zauner G., Haslhofer M., Pree R. Quantitative determination of porosity by active thermography; Proceedings of the Review of Quantitative Non-destructive Evaluation; Portland, OR, USA. 30 July–4 August 2007; pp. 702–708.
Ibarra-Castanedo C., "Quantitative subsurface defect evaluation by Pulsed Phase thermography: Depth Retrieval with the Phase", PhD thesis. Facultè des sciences et de Gènie Universitè Laval Québec, (2005).
Maldague X (1993). In: 1 (ed) Non-destructive Evaluation of Materials by Infrared Thermography. Springer, London.
Maldague X., Galmiche F., Ziadi A., "Advances in pulsed phase thermography", Infrared Physics & Technology, Vol. 43, 175-181 (2002).
Maldague X., Theory and Practice of Infrared Technology for Non-Destructive Testing, Wiley, New York, (2003).
Mallick P.K., "Fiber-Reinforced Composites: Materials, Manufacturing and Design," CRC Press, Taylor & Francis Group, 2008.
Mayr G. and Handorfer G., "Porosity determination by pulsed Thermography in reflection mode", in Proceedings of the 10th International Conference on Quantitative InfraRed Thermography, Québec, Canada, July 2010.
Roth D., Bodis J., Bishop C. (1997) Thermographic imaging for high-temperature composite materials a defect detection study. J Res Nondestruct Eval 9(3):147–169.
Sun J (2006) Analysis of pulsed thermography methods for defect depth prediction. J Heat Transf 128(4):329–338.
Susa M., Maldague X., Boras I., "Improved method for absolute thermal contrast evaluation using Source Distribution Image (SDI)", Infrared Physics & Technology, 53-3, 197-203, (2010).